Posted on 22 Nov 2022 — The copyright holder is the author/funder. All rights reserved. No reuse without permission. — https://doi.org/10.1002/essoar.10505010.1 — This a preprint and has not been peer reviewed. Data may be preliminary.

Different trends in Antarctic temperature and atmospheric CO2 during the last glacial

Peisong Zheng[1], Joel Pedro[2], Markus Jochum[3], Sune Olander Rasmussen[4], and Zhongping Lai[5]

[1]Guangdong Provincial Key Laboratory of Marine Biotechnology, Institute of Marine Sciences, Shantou University
[2]University of Tasmania
[3]University of Copenhagen
[4]Centre for Ice and Climate, Section for the Physics of Ice, Climate, and Earth, Niels Bohr Institute, University of Copenhagen
[5]Institute of Marine Sciences, Shantou University

November 22, 2022

Abstract

Using Antarctic ice-core records, we determine for each Antarctic Isotope Maximum (AIM) of Marine Isotope Stage 3 (MIS-3: ca. 28,000 to 59,000 years before present) the rates and durations of warming and atmospheric CO_2 rise. We find that the AIM warming rates significantly decrease as the climate cools from early to late MIS-3. In contrast, the rate of CO_2 rise during AIMs shows no significant trend across this interval. We further find that the AIM warming rate is not sensitive to Heinrich (H) events, contrasting with CO_2, which rises for significantly longer time (compared to the temperature rise) during AIMs which coincide with H events. These distinct Antarctic temperature and CO_2 responses to varying background climate and H events challenge the view that millennial-scale CO_2 and Antarctic temperature changes are dominated by the same physical processes, suggesting an important contribution of low-to-mid-latitude processes to the CO_2 rises.

Different trends in Antarctic temperature and atmospheric CO_2 during the last glacial

Peisong Zheng[1, 2], Joel B. Pedro[3,4], Markus Jochum[5], Sune O. Rasmussen[6], Zhongping Lai[1, 7 *]

[1] Guangdong Provincial Key Laboratory of Marine Biotechnology, Institute of Marine Sciences, Shantou University, Shantou 515063, China.

[2] School of Earth Sciences, China University of Geosciences, Wuhan 430074, China.

[3] Australian Antarctic Division, Kingston, Tasmania, Australia.

[4] Australian Antarctic Program Partnership, University of Tasmania, Hobart, Tasmania, Australia.

[5] TeamOcean, Niels Bohr Institute, University of Copenhagen, Copenhagen, Denmark.

[6] Centre for Ice and Climate, Section for the Physics of Ice, Climate, and Earth, Niels Bohr Institute, University of Copenhagen, Copenhagen, Denmark.

[7] Three Gorges Research Center for Geohazards of MOE, China University of Geosciences, Wuhan 430074, China.

Corresponding author: **Zhongping Lai** (zhongping.lai@yahoo.com)

Key Points:

- The Antarctic warming rate during Antarctic Isotope Maxima significantly decreased as the climate cooled toward the glacial maximum.
- The Antarctic warming rate during Antarctic Isotope Maxima is insensitive to whether the warming coincides with a Heinrich event.
- In contrast, the millennial-scale CO_2 rise is insensitive to long-term glacial cooling but sensitive to the presence of Heinrich events.

Abstract

Using Antarctic ice-core records, we determine for each Antarctic Isotope Maximum (AIM) of Marine Isotope Stage 3 (MIS-3: ca. 28,000 to 59,000 years before present) the rates and durations of warming and atmospheric CO_2 rise. We find that the AIM warming rates significantly decrease as the climate cools from early to late MIS-3. In contrast, the rate of CO_2 rise during AIMs shows no significant trend across this interval. We further find that the AIM warming rate is not sensitive to Heinrich (H) events, contrasting with CO_2, which rises for significantly longer time (compared to the temperature rise) during AIMs which coincide with H events. These distinct Antarctic temperature and CO_2 responses to varying background climate and H events challenge the view that millennial-scale CO_2 and Antarctic temperature changes are dominated by the same physical processes, suggesting an important contribution of low-to-mid-latitude processes to the CO_2 rises.

Plain Language Summary

Glacial climate is characterized by millennial-scale variations in polar temperature and atmospheric CO_2 concentration. Over the last two decades, a consistent explanation of the temperature changes has emerged, but no such consensus exists with regard to CO_2. However, due to the similarity of their records it is frequently proposed that CO_2 and Antarctic temperature were controlled by the same processes. Here we present a new analysis of millennial-scale Antarctic warming and CO_2 rise based on ice-core data. Our results show that during the latter half of the glacial period, the Antarctica warming rate decreased as the climate cooled, but it was not affected by occasional massive iceberg discharges (known as Heinrich events) that had a dramatic impact on northern hemisphere climate. On the other hand, the rate of CO_2 change was

insensitive to the glacial cooling trend, but the CO_2 rise was sensitive to the occurrence of Heinrich events. This suggests that on top of the processes that control millennial-scale Antarctic temperature variations and also play a role for CO_2 levels, there are other processes (possibly of extra-polar or terrestrial origin) that are important for the CO_2 dynamics.

1 Introduction

Antarctic Isotope Maximums have a systematic relationship with the Dansgaard-Oeschger (DO) oscillations recorded in Greenland ice cores during the last glacial period (EPICA, 2006). The cold (Greenland stadial: GS) phase of the DO oscillation in Greenland coincides with AIM warming in Antarctica and the warm (Greenland interstadial: GI) phase of the DO coincides with AIM cooling (Figure 1). According to the bipolar ocean seesaw hypothesis (Stocker & Johnsen, 2003), this interhemispheric coupling results from changes in northward heat transport by the Atlantic Meridional Overturning Circulation (AMOC): GSs are associated with a weak AMOC, reduced northward heat transport in the Atlantic and warming in the South Atlantic. AIM warming in Antarctica follows, after a centennial-scale lag, as the South Atlantic warm anomaly spreads through the upper to intermediate-depth ocean and is gradually mixed across the Antarctic Circumpolar Current, in turn melting back Southern Ocean sea ice and increasing atmospheric heat transport to Antarctica (see Pedro et al., 2018; for a view that places more emphasis on buoyancy forcing see Thompson et al., 2019).

Previous work, based on the EPICA Dronning Maud Land (EDML) ice core, identified a strong linear relationship ($r^2 = 0.85$) between the duration of GSs and the amplitude of corresponding AIMs during MIS-3 (EPICA, 2006). The linear relationship suggested that the amplitude of AIM warming depends only on the duration of Greenland stadials and that the operation of the bipolar seesaw is not significantly influenced either by the evolution of the

climate state during the glacial, nor by the presence of H events. However, only eleven of the sixteen MIS-3 AIMs were considered in that analysis and more recent studies propose that the bipolar seesaw is sensitive to background climate (Capron et al., 2010; Margari et al., 2010), and the presence of H events (Margari et al., 2010). However, these sensitivities have not previously been quantified or statistically assessed.

The apparent similarity between atmospheric CO_2 concentrations (hereafter CO_2) and Antarctic temperature change in the Antarctic ice-core record (Figure 1) has been hypothesized to result from a common cause, such as changes in wind-driven upwelling (Anderson et al., 2009; Anderson & Carr, 2010; Menviel et al., 2018; Toggweiler et al., 2006), or changes in the formation of Antarctica Bottom Water (AABW, Menviel et al., 2015). In both cases, the release of CO_2 and heat involve coupled Southern Ocean processes: increased ventilation of relatively warm and carbon-rich sub-surface waters in the Southern Ocean (Bauska et al., 2018; Gottschalk et al., 2019; Jaccard et al., 2016; Skinner et al., 2020); and/or increased poleward heat transport accompanying the AABW formation and CO_2 ventilation (Menviel et al., 2015). However, there are two obvious differences between the millennial-scale CO_2 and Antarctic temperature changes: a) CO_2 maximums associated with Heinrich stadials (HS, defined here as GS containing a H event) visibly lag the peak of the corresponding AIM events (Figure 1; Bereiter et al., 2012); and, b) CO_2 rises during non-Heinrich stadials (nHS), if resolved at all, are thought to be of lower amplitude than those during HS (Ahn & Brook, 2014). However, as with the sensitivity of AIM warming to background climate and H events, a robust statistical assessment of these CO_2 features is lacking. Thus, we constrain for each MIS-3 AIM the amplitude and duration of the AIM warming phase and CO_2 rise. We then test the sensitivities of AIM warming and CO_2 rise to the changes in background climate state and the presence of H events.

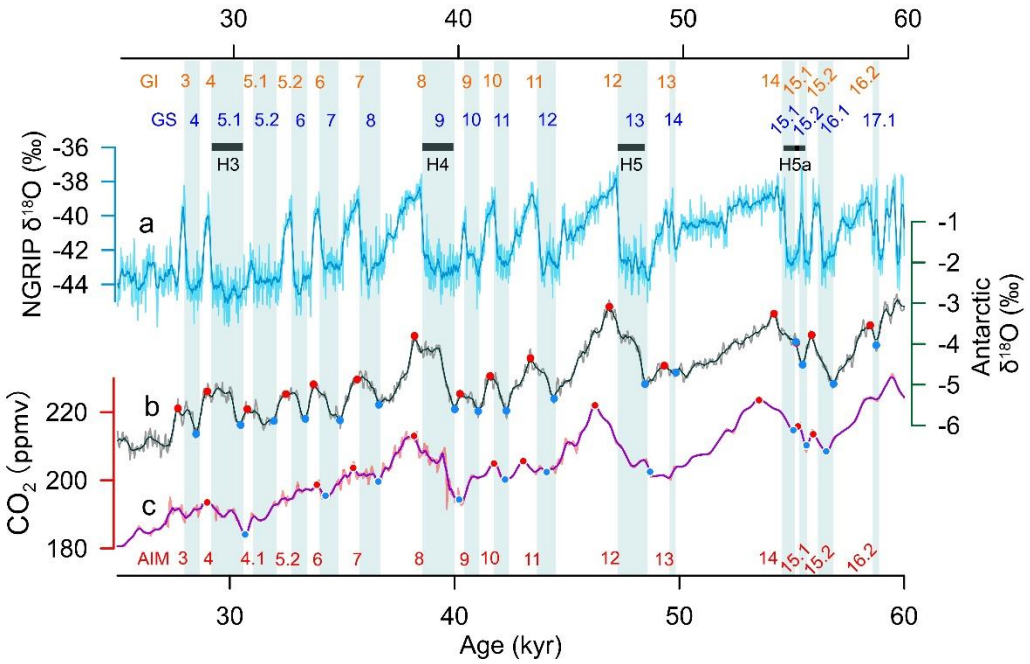

Figure 1. Millennial-scale climate events and atmospheric CO_2 variations for the MIS-3. a. The oxygen isotope ratio ($\delta^{18}O$) from the North Greenland Ice Core Project (NGRIP) ice core, as a proxy for Greenland temperature (NGRIP, 2004; Svensson et al., 2008)**. b.** The Antarctic five-core averaged $\delta^{18}O$ record (Buizert et al., 2018). **c.** The composite Antarctic ice core CO_2 record (Bereiter et al., 2012). The red and blue dots in **b** and **c** show the identified AIM and CO_2 maximums and minimums (see text for definitions). **b** is on the WD2014 timescale, all other records were transferred to the WD2014 time scale by stretching the GICC05/AICC2012 age to 1.0063 times (Buizert et al., 2015). The Greenland stadials and interstadials events are numbered following Rasmussen et al. (2014), the timing of Greenland climate transition is from Buizert et al. (2015) and WAIS (2015). Timespan of the H events are marked by the horizontal gray bars. The AIM event number is following EPICA (2006) and extended to AIM 16.2.

2 Methods and results

2.1. AIM temperature rise

We use the recently published Antarctic five-core averaged $\delta^{18}O$ stack (in WD2014 timescale; Buizert et al., 2014) to determine the individual MIS-3 AIM warming amplitudes. To exclude uncertainties associated with $\delta^{18}O$-temperature transformation (Jouzel et al., 2013; Landais et al., 2015), we use per mille (‰) $\delta^{18}O$ change as our unit of measure for AIM warming amplitude. EPICA (2006) concludes that AIM warming amplitude is only controlled by the duration of the corresponding GS; i.e. that the AIM warming rate is constant. To test this result, we go a step further than EPICA (2006) and define here the AIM amplitude divided by the GS duration as the bipolar seesaw (BPS) warming. The GS durations are obtained from previous work (Buizert et al., 2015).

To obtain a robust estimate for the bipolar seesaw warming rate and its uncertainty, a Monte Carlo (MC) Methods is used: in every iteration, the maximums and minimums of each AIM are determined from a randomly perturbed version of the five-core averaged $\delta^{18}O$ record which is smoothed with a 200-yr moving average before calculating the BPS warming rate of each AIM. The randomly perturbed $\delta^{18}O$ record is created by drawing values from the normal distribution of the five-core averaged $\delta^{18}O$ record with standard deviation set at 0.12‰ (found as the standard deviation of the residual of the smoothed data relative to the unsmoothed one). Considering the 100 to 200 yr lag of the onsets and ends of AIM events relative to Greenland GS and GI transitions (Svensson et al., 2020; WAIS, 2015), we conservatively search for the isotope maximums and minimums in a 300 yr window starting at the time of the corresponding Greenland climate transition (the window is not allowed to cross the adjacent Greenland climate

126 transition). After 100,000 iterations the median BPS warming rate for each AIM is used as the
127 output (Figure 2a), and the 95% confidence interval (CI) of the MC generated rates of each AIM
128 is used as the estimate of uncertainty range.

129 In contrast to the results of EPICA (2006), we do not observe a strong linear correlation
130 between GS duration and AIM amplitude (Figure 2a). Instead, our data suggest a lower BPS
131 warming rate during late MIS-3 than during early MIS-3 (Figure 2a, S1). To test if this reduction
132 is systematic, we plot the BPS warming rates against the AIM ages (defined as the onset of the
133 corresponding Greenland stadial). A clear decline in the warming rate across MIS-3 is observed
134 (Figure 2b). The significance of the observed slope is evaluated by comparing it with the slopes
135 generated from randomly permuting the BPS warming rate data points (keeping the AIM ages)
136 and re-calculating the resulting slopes 100,000 times. Only 0.06% of the absolute value of the
137 randomly generated slopes are larger than that obtained from the actual data (Figure 2c),
138 demonstrating the declining trend of BPS warming rate during MIS3 is significant.

139 Following EPICA (2006), our analysis above assumes that the BPS warming rate is
140 linear. If the AIM warming instead rises asymptotically, as predicted by the "minimum
141 thermodynamic seesaw model" (Margari et al., 2010; Stocker & Johnsen, 2003), then our
142 definition of the BPS warming rate could be biased low for longer GS. To test whether our result
143 holds under the assumption of an asymptotic rather than linear temperature increase during AIMs
144 we repeat our analysis fitting the warming phase of each AIM using the minimum
145 thermodynamic seesaw model (Stocker & Johnsen, 2003; Figure S2): $\Delta T_S=\Delta T_N(e^{-t/\tau}-1)$, where
146 ΔT_S and ΔT_N are the amplitude of southern warming and northern cooling respectively, t is the
147 time since the start of the stadial, and τ is the equilibration timescale of the seesaw system,
148 estimated as 1120 yr (Margari et al., 2010; Stocker & Johnsen, 2003). We use isotope units

rather than temperature, and introduce the constant $-T_G$ to replace ΔT_N, representing the amplitude of northern temperature (isotope) drop that gives the best fit to the observed AIM isotope growth rate (note the $-T_G$ and ΔT_N have opposite sign). With τ kept constant, the shape of the fitted curve is determined by $-T_G$, with smaller $-T_G$ corresponding to slower rises (Figure S3). Similar to the linear case, Monte Carlo Methods is applied, and $-T_G$ of each AIM is determined as the median of 100,000 iterations (Figure 2d).

Like the linear assessment of BPS warming rate, a slope showing the decline of $-T_G$ toward the glacial maximum is observed (Figure 2d). To test the significance of the slope, we randomly permute the $-T_G$ values and re-calculate the slope 100,000 times and find that the absolute value of the random slopes is larger than the value found from data in only 4.9% of the cases, (Figure 2e), suggesting that $-T_G$ has a significant trend during MIS-3. This could be due to a weakening of efficiency of the bipolar seesaw or a reduction of the driving ΔT_N, but as the latter is not found in the reconstruction of northern temperature (Kindler et al., 2014), we conclude that the bipolar seesaw was indeed weakening significantly during MIS-3 both under the Stocker and Johnsen (2003) minimum thermodynamic seesaw model and that of linear AIM warming rates (EPICA, 2006).

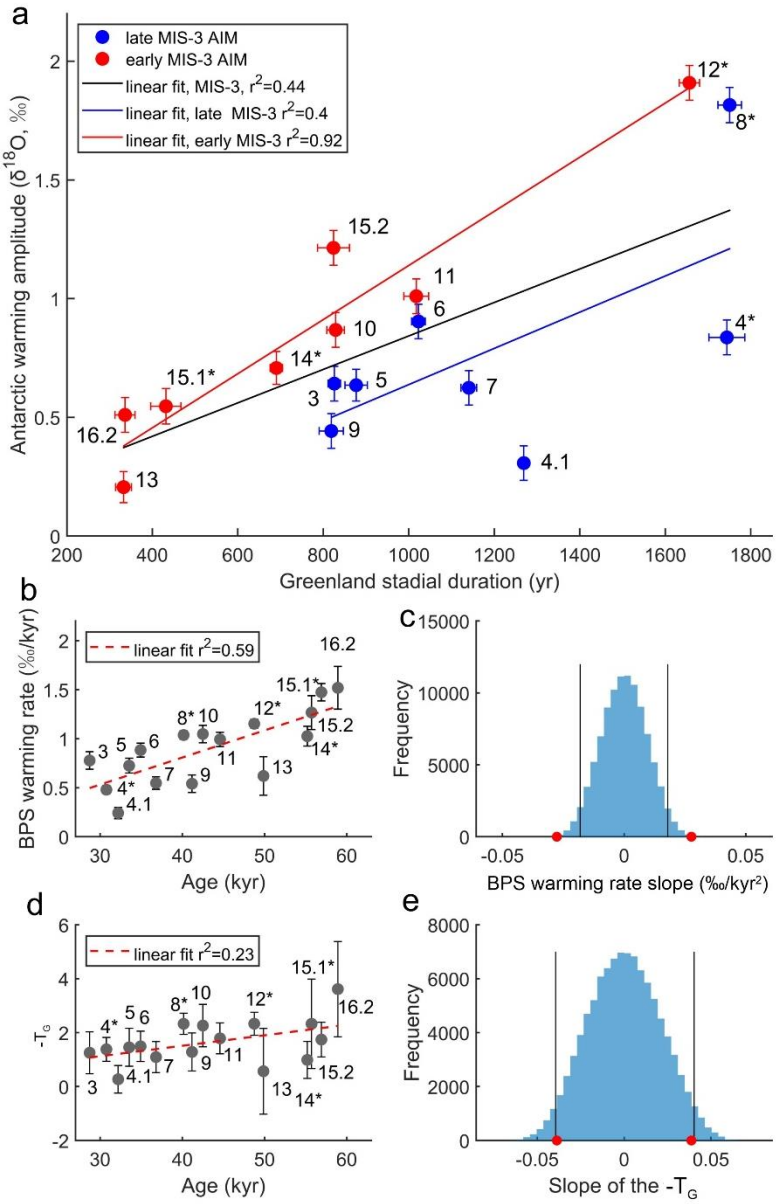

165

166 **Figure 2. The BPS warming rate results. a.** Greenland stadial duration and Antarctic warming
167 amplitude, the AIM nomenclature is following EPICA (2006) and has been extended to AIM
168 16.2. The error bar shows the uncertainty of GS duration (Buizert et al., 2015; WAIS, 2015) and
169 the 95% CI of the amplitude. **b.** The BPS warming rate plotted against the age of the AIM. The
170 error bar shows the range of 95% CI. **c.** The distribution of the slopes of the randomly permuted
171 BPS warming rates, the red circle marks ±1 time the slope observed from **b**, the 2.5% and 97.5%

fractile of the randomly generated slope are marked by vertical black lines. **d, e.** The same as **b, c** for $-T_G$ instead of the BPS warming rate.

To test the sensitivity of AIM warming to H events we group the BPS warming rates and $-T_G$ values for each AIM into HS and nHS categories (Figure S1). A Student's t-test shows no significant difference (at 95% significance level) between HS and nHS BPS warming rates or $-T_G$. These results suggest that the processes controlling Antarctic warming are insensitive to the H events.

Our result of a weakening bipolar seesaw during MIS-3 is robust to replacing Greenland stadial durations with the duration of the corresponding Antarctic isotope rise (the time between the identified isotope minimum and maximum, Table S1). Removing the long-term signal represented by 20,000 yr smoothing of the five-core averaged isotope data also does not change the conclusions (Table S1, Figure S4). We also carried out the analysis of the BPS warming rate and $-T_G$ on the individual ice-core records going into the five-core averaged data set: West Antarctic Ice Sheet Divide (WDC; WAIS, 2013, 2015), European Project for Ice Coring in Antarctica (EPICA) in the interior of Dronning Maud Land (EDML; EPICA, 2006), Talos Dome (Landais et al., 2015; Stenni et al., 2011), EPICA Dome C (EDC; EPICA 2004), and Dome Fuji (Fuji; Kawamura et al., 2007; Watanabe et al., 2003). Similar results are obtained (Table S1, Figure S4). Although the EDML record may reflect more low-latitude and atmospheric signals (Landais et al., 2015), our results show that in terms of the overall bipolar seesaw response, it is not systematically different from other Antarctic ice cores. This is consistent with the conclusion that a spatially homogeneous oceanic component of the AIM events related to the

thermodynamic seesaw response is the first and dominant principle component of the AIM variability (Buizert et al., 2018).

2.2. Millennial CO_2 rise:

We determine the amplitude of MIS-3 millennial-scale CO_2 rise using the composite CO_2 record (on the AICC2012 timescale; Bereiter et al., 2015; Figure 1, S5). The MIS-3 section of the composite CO_2 record consists of the Siple Dome (20 to 40 kyr BP; Ahn & Brook, 2014) and Talos Dome (40 to 60 kyr BP; Bereiter et al., 2012) records. To avoid the influence of different gas smoothing between ice cores, the CO_2 data is smoothed using a 300 yr moving average, which is larger than the mean resolution of both CO_2 records (96 and 246 for Siple and Talos Dome respectively). We note that there is a systematic offset between the two CO_2 records (Bereiter et al., 2012) with a junction point (at about 40 kyr BP, Figure S5), this offset does not fall within a period of assessed CO_2 rise, so it does not affect any of our derived CO_2 amplitudes.

Considering the CO_2 peak could lag the abrupt DO warming by several hundred to a thousand years (Bereiter et al., 2012; Figure S5), we here extend the search window for the CO_2 maximums and minimums to 100 yr prior and 1000 yr after the Greenland climate transition. We use the timing of Greenland climate transitions defined in Greenland $\delta^{18}O$ and Ca+ data (Rasmussen et al., 2014).

In calculating the amplitudes and rates of MIS-3 CO_2 rise, we assess only those CO_2 rises with amplitudes significantly larger than the measurement uncertainty (at the 95% level, Figure S6). A total ten CO_2 rise are identified, five for the HS (DO 4, 8, 12, 14, 15.1) and five for the nHS periods (DO, 6, 7, 10, 11, 15.2, Figure 1, 3a). We here focused on the overall CO_2 response

and defined the rate of CO_2 rise (Figure 3b) as CO_2 amplitude divided by the duration of the rise. The CO_2 rate and its uncertainty are estimated by similar MC method of temperature rates.

In contrast to AIM warming rates, we do not find evidence for a significant decline in the rate of CO_2 rise across the MIS-3 AIM events (with two-side significance 82.7%, Figure 3c). Note that this result is not a statistical artifact due to the low number of CO_2 events resolved by the data, see a one-to-one comparison using only events both analysed in the CO_2 and temperature records in Figure S7. However, the bubble enclosure characteristics of different ice core sites (Bereiter et al., 2012) and the depth/age-dependent ice diffusion (Ahn et al., 2008) could unevenly smooth the composite CO_2 records and bias the CO_2 amplitude. To test the influence of these effects, we perform additional tests and compared the CO_2 and temperature trends for the Talos section of composite CO_2 (Bereiter et al., 2012) vs the Talos $\delta^{18}O$ data (Landais et al., 2015; Stenni et al., 2011; Supporting Information, Figure S8), and for the newly recovered EDC CO_2 record (Nehrbass-Ahles et al., 2020) spanning 330 to 440 kyr BP vs the EDC δD data (EPICA, 2004), (Supporting Information, Figures S9 and S9). In both cases, the CO_2 trend is less significant than the Antarctic temperature trend (Figure S8, S9). The above experiments are also designed to consider the influence of using different timescales and changes in delta-age (age difference between gas and ice at the same depth, see Supporting Information). The results show that our conclusions are not sensitive to these factors (Supporting Information, Figure S8, S9).

Our results are cross-validated by another method that compares the CO_2 and temperature trend: we let the CO_2/temperature rates randomly varying within their uncertainty and repeatedly calculate the slope (without permuting the CO_2/temperature rate data points), after 100,000 iterations it turn out the median temperature rate slopes are larger than the CO_2 rate slopes in all

238 CO_2–temperature comparison cases (Five-core $\delta^{18}O$ vs composite CO_2; Talos CO_2 vs the Talos
239 $\delta^{18}O$; new EDC CO_2 vs the EDC δD, Supporting Information, Figure 3e, 3f, S11). Overall, these
240 results suggest the rate of CO_2 rise is less sensitive to varying background climate across the
241 MIS-3 than the Antarctic temperature trend.

242 We also do not find a significant difference between the rate of CO_2 rise during HS and
243 nHS (t-test with 95% significance level). However, we do find, consistent with previous work
244 (Bereiter et al., 2012), that CO_2 rise 'overshoots' (the excess CO_2 rise time relative to
245 corresponding GS duration) are longer during HS than during nHS (median HS overshoot: 307
246 yr, nHS: -126 yr, Figure 3d). A t-test confirms that the longer overshoots for HS CO_2 rise relative
247 to nHS are significant (at the 95% level). For comparison, we determine the Antarctic warming
248 overshoot in the same way, and no significant difference between HS and nHS is detected (at
249 95% significance level, Figure S1), consistent with a stable north to south lag (Svensson et al.,
250 2020; WAIS, 2015).

251 The CO_2 sensitivity to background climate and H events are similar when detrended CO_2
252 data (removing the long-term signal represented by 20,000 yr smoothing) are used (Supporting
253 Information, Figure S5, S12). To compare with previous research, we also determined the
254 maximums/minimums from a spline fitted CO_2 data with cut off period of 500 yr (Bereiter et al.,
255 2012), again the results hold (Supporting Information, Figure S5, S12).

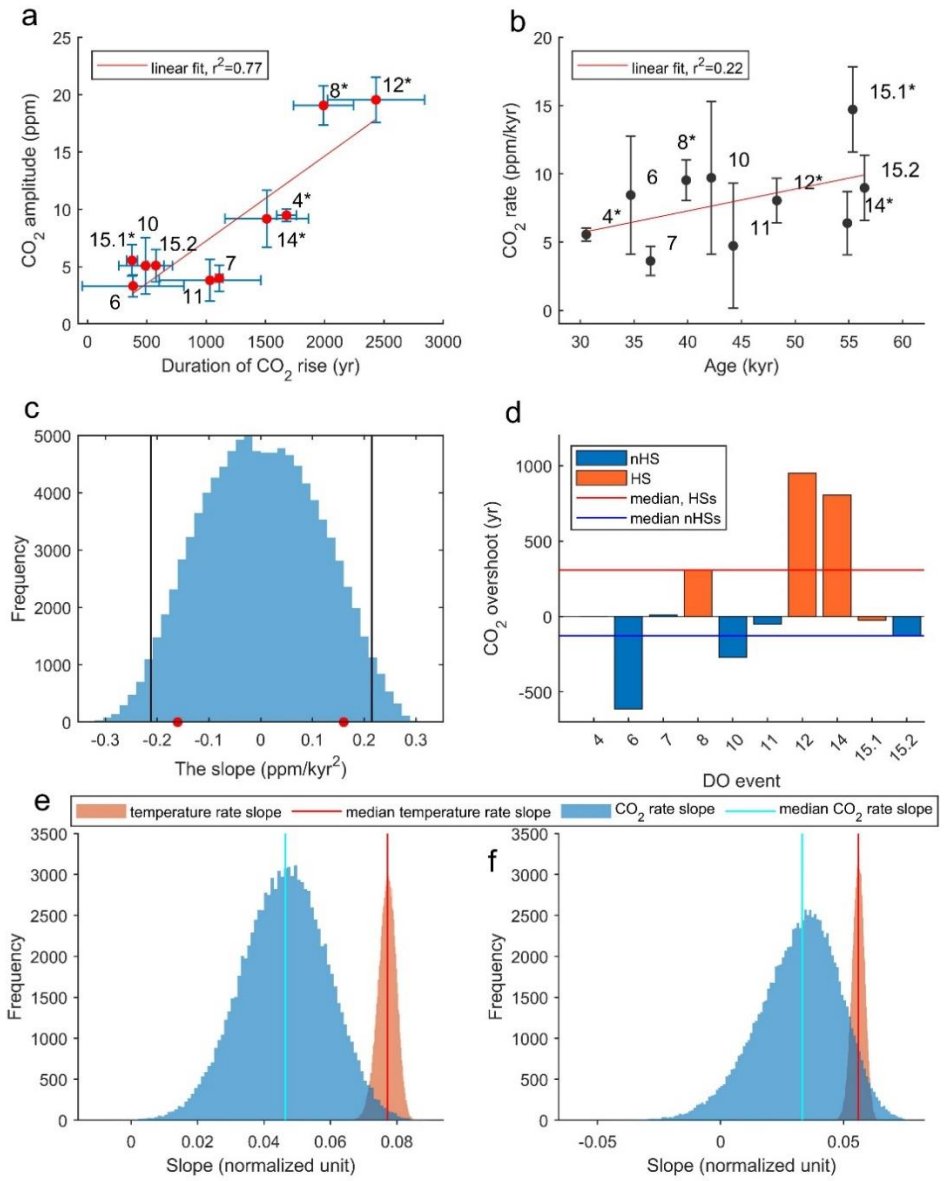

Figure 3. The CO_2 rates and CO_2 overshoot. a. The CO_2 amplitude vs the duration of CO_2 rises, the error bar marks the 95% CI of the amplitude and duration. **b.** CO_2 rate vs the age of the CO_2 rise, which is defined by the initiation of the corresponding Greenland stadial. The error bar marks the 95%CI. **c.** The comparison between the ±1 time observed CO_2 slope in **b** (red dots) with the slopes generated by randomly permuting the CO_2 rate. The 2.5% and 97.5% fractile of the randomly generated slope is marked by vertical black lines. **d.** The CO_2 overshoot. **e.** The

distribution of the randomly generated CO_2/temperature rate slopes of five-core averaged $\delta^{18}O$ data (Buizert et al., 2018) and the composite CO_2 data (Bereiter et al., 2015). Note the rates are normalized before fitting the slope. **f.** same as **e** but for the new EDC CO_2 (Nehrbass-Ahles et al., 2020) and EDC δD data (EPICA, 2004).

3 Discussion

3.1. Interpreting the temperature sensitivity

Our statistical analysis suggests the AIM temperature response to the DO cycles is gradually weakened throughout the MIS-3. This result provides a firm quantitative basis for previous suggestions of weakened bipolar connections when climate approaches the glacial maximum (Margari et al., 2010; Mcmanus et al., 1999; Wolff et al., 2009).

Recent work indicates that the majority of AIM variability (about 83%) can be explained by a spatially homogeneous oceanic mode (Buizert et al., 2018) that is well captured by the minimum thermodynamic seesaw model (Stocker & Johnsen, 2003). The reduction of the BPS warming rate and $-T_G$ as the climate state cools suggest either a weakening of the mechanisms coupling Antarctic temperature to this oceanic mode and/or a weakening influence of the DO cycles on the Southern Ocean itself. Performing a similar analysis to ours on AIM warming rates observed on surface temperature reconstructions from Southern Ocean marine sediment cores may resolve which is the case.

A recent coupled-model investigation of the bipolar seesaw mechanism (Pedro et al., 2018) suggested that during Greenland stadials, the weakened AMOC drives Antarctic warming

284 through the following chain of events: Reduced northward advection of heat in the Atlantic
285 Ocean results in heat accumulation in the South Atlantic. This heat then spreads east around the
286 globe along the northern edge of the Antarctica Circumpolar Current (ACC). As a result, the
287 temperature gradient across the ACC increases, driving an increase in the cross-ACC heat flux
288 carried by ocean eddies. Temperature anomalies south of the ACC are amplified by the retreat of
289 sea ice and the resulting ice-albedo feedback. Finally, heat from the Southern Ocean sea-ice zone
290 is transported to Antarctica by atmospheric eddies, i.e., storms.

291 A cooler background climate state of late MIS-3 (as shown by Antarctic water isotope
292 records (Buizert et al., 2018), or similar trend in ice core noble gas estimates of mean ocean
293 temperature; Bereiter et al., 2018), with thicker Antarctic sea ice, would be expected to reduce
294 the BPS warming rate, because thicker ice would inhibit the ice-albedo feedback (Levermann et
295 al., 2007). Moreover, the concurrent expansion of the sea ice expected in a colder climate would
296 lower the efficiency of atmospheric heat transportation from the warm sea-ice zone to Antarctica,
297 due to the greater distance between Antarctic and the sea-ice-free area. Indeed, marine sediment-
298 core (Collins et al., 2012; Gersonde et al., 2005; Stuut et al., 2004), WDC sea-salt Na record
299 (WAIS, 2015), and climate model (Ferrari et al., 2014), show evidence for Southern Ocean sea-
300 ice expansion at the end of glacial periods.

301

302 **3.2. Interpreting the CO_2 sensitivity**

303 Our results suggest that in contrast to changes in Antarctic temperature the millennial-
304 scale CO_2 rises show little, if any, sensitivity to varying background climate during MIS-3. Our
305 results also show that this less background state-dependent response of CO_2 is also observed in

earlier glacial periods (Nehrbass-Ahles et al., 2020; Figure S9), which suggests it is a robust feature of millennial climate variability during glacial periods. Recent studies have suggested that increased Southern Ocean deep convection can jointly explain AIM warming and CO_2 trends via the ventilation of heat and CO_2 from ocean depths (Menviel et al., 2018; Skinner et al., 2020). Carbon reservoir age and deep-water temperature reconstructions from the South Atlantic appear to support this 'Southern Ocean hypothesis' during HS-4 (Skinner et al., 2020), but do not quantify the scale of its contribution. Furthermore, although strengthened winds are often invoked as the forcing for increased upwelling, Southern Ocean eddies may partially or fully nullify the influence of wind changes on upwelling (Munday et al., 2013). Our results on the different sensitivities of AIM temperature trends and CO_2 to background climate state challenge that a single physical process dominates the millennial signals in both throughout MIS-3. Instead, a dominant influence of Southern Ocean processes on the AIM temperature evolution (Buizert et al., 2018; Pedro et al., 2018) and an important contribution of low- and mid-latitude processes to CO_2, for example by reduction of the biological pump (Nielsen et al., 2019), or CO_2 release from terrestrial sources (Bauska et al., 2016; Marcott et al., 2014; Rhodes et al., 2015), would appear consistent with our results.

Alternately, the Southern Ocean hypothesis could sidestep our observational constraint if the ventilation of ocean heat is reduced relative to the CO_2 as MIS-3 progresses and the climate cools, or if heat ventilated by deep convection has less influence on Antarctic temperature due, for example, to expanded Antarctic sea ice (Collins et al., 2012; Gersonde et al., 2005; Stuut et al., 2004). In either case, our observations provide a new target for model studies seeking to replicate the millennial-scale variability of temperature and CO_2 and their sensitivities to climate state and H events.

The most obvious decoupling of CO_2 and Antarctic temperature occurs during the centennial-scale CO_2 overshoots accompanying H events (Figure 3d). While the CO_2 overshoots are still unexplained, there are a number of candidate mechanisms that would be expected to express a signal in CO_2 and not in Antarctic temperature. Notably, rapid ventilation of accumulated respired carbon from intermediate-depth Atlantic (Chen et al., 2015; Jaccard et al., 2016) and again reduction of the biological pump (Nielsen et al., 2019), or terrestrial CO_2 release (Bauska et al., 2016; Marcott et al., 2014; Rhodes et al., 2015).

Acknowledgments, Samples, and Data

This work was funded by the Natural Science Foundation of China (Grant No. 41290252). JBP and SOR acknowledges support from a Carlsberg Foundation grant to project ChronoClimate. We thank Christo Buizert and Xu Zhang for discussions. ZL and PZ proposed the research. PZ conducted the analyses with support from JBP, MJ and SOR. All authors contributed to the writing of manuscript. The WDC, EDC, EDML, Fuji, Talos $\delta^{18}O$ in WD2014 timescale, and the five-core averaged $\delta^{18}O$ data are included in this paper (and its supplementary information files): Buizert, C., Sigl, M., Severi, M., Markle, B. R., Wettstein, J. J., McConnell, J. R., . . . Kawamura, K. (2018). Abrupt ice-age shifts in southern westerly winds and Antarctic climate forced from the north. *Nature*, *563*(7733), 681-685. The composite CO_2 data is included in this paper (and its supplementary information files): Bereiter, B., Eggleston, S., Schmitt, J., Nehrbass Ahles, C., Stocker, T. F., Fischer, H., . . . Chappellaz, J. (2015). Revision of the EPICA Dome C CO_2 record from 800 to 600 kyr before present. *Geophysical Research Letters, 42*(2), 542-549. The new EDC CO_2 data is included in this paper (and its supplementary information files):

Nehrbass-Ahles, C., Shin, J., Schmitt, J., Bereiter, B., Joos, F., Schilt, A., . . . Grilli, R. (2020). Abrupt CO_2 release to the atmosphere under glacial and early interglacial climate conditions. *Science, 369*(6506), 1000-1005. The EDC δD data is included in this paper (and its supplementary information files): EPICA. (2004). Eight glacial cycles from an Antarctic ice core. *Nature, 429*(6992), 623-628.

References

1. Ahn, J., & Brook, E. J. (2014). Siple Dome ice reveals two modes of millennial CO2 change during the last ice age. *Nature Communications, 5*(4), 4723.
2. Ahn, J., Headly, M., Wahlen, M., Brook, E. J., Mayewski, P. A., & Taylor, K. C. (2008). CO 2 diffusion in polar ice: observations from naturally formed CO 2 spikes in the Siple Dome (Antarctica) ice core. *Journal of Glaciology, 54*(187), 685-695.
3. Anderson, R. F., Ali, S., Bradtmiller, L. I., Nielsen, S. H., Fleisher, M. Q., Anderson, B. E., & Burckle, L. H. (2009). Wind-driven upwelling in the Southern Ocean and the deglacial rise in atmospheric CO2. *Science, 323*(5920), 1443-1448.
4. Anderson, R. F., & Carr, M.-E. (2010). Paleoclimate. Uncorking the Southern Ocean's vintage CO2. *Science, 328*(5982), 1117-1118.
5. Bauska, T. K., Baggenstos, D., Brook, E. J., Mix, A. C., & Lee, J. E. (2016). Carbon isotopes characterize rapid changes in atmospheric carbon dioxide during the last deglaciation. *Proc Natl Acad U S A, 113*(13), 3465-3470.
6. Bauska, T. K., Brook, E. J., Marcott, S. A., Baggenstos, D., Shackleton, S., Severinghaus, J. P., & Petrenko, V. V. (2018). Controls on Millennial-Scale Atmospheric CO2 Variability During the Last Glacial Period. *Geophysical Research Letters, 45*(15), 7731-7740. doi:10.1029/2018GL077881

7. Bereiter, B., Eggleston, S., Schmitt, J., Nehrbass Ahles, C., Stocker, T. F., Fischer, H., . . . Chappellaz, J. (2015). Revision of the EPICA Dome C CO2 record from 800 to 600 kyr before present. *Geophysical Research Letters*, *42*(2), 542-549.
8. Bereiter, B., Lüthi, D., Siegrist, M., Schüpbach, S., Thomas F, S., & Fischer, H. (2012). Mode change of millennial CO2 variability during the last glacial cycle associated with a bipolar marine carbon seesaw. *Proceedings of the National Academy of Sciences of the United States of America*, *109*(25), 9755-9760.
9. Bereiter, B., Shackleton, S., Baggenstos, D., Kawamura, K., & Severinghaus, J. (2018). Mean global ocean temperatures during the last glacial transition. *Nature, 553*(7686), 39-44.
10. Buizert, C., Cuffey, K. M., Severinghaus, J. P., Baggenstos, D., Fudge, T. J., Steig, E. J., . . . Brook, E. J. (2015). The WAIS Divide deep ice core WD2014 chronology – Part 1: Methane synchronization (68–31 ka BP) and the gas age–ice age difference. *Climate of the Past*, *11*(4), 153-173.
11. Buizert, C., Sigl, M., Severi, M., Markle, B. R., Wettstein, J. J., McConnell, J. R., . . . Kawamura, K. (2018). Abrupt ice-age shifts in southern westerly winds and Antarctic climate forced from the north. *Nature*, *563*(7733), 681-685.
12. Capron, E., Landais, A., Chappellaz, J., Schilt, A., & Stenni, B. (2010). Millennial and sub-millennial scale climatic variations recorded in polar ice cores over the last glacial period. *Climate of the Past Discussions*, *6*(1), 345-365.
13. Chen, T., Robinson, L. F., Burke, A., Southon, J., Spooner, P., Morris, P. J., & Ng, H. C. (2015). Synchronous centennial abrupt events in the ocean and atmosphere during the last deglaciation. *Science, 349*, 1537-1541.
14. Collins, L. G., Pike, J., Allen, C. S., & Hodgson, D. A. (2012). High - resolution reconstruction of southwest Atlantic sea - ice and its role in the carbon cycle during marine isotope stages 3 and 2. *Paleoceanography*, *27*(3), PA3217.
15. EPICA. (2004). Eight glacial cycles from an Antarctic ice core. *Nature*, *429*(6992), 623-628.
16. EPICA. (2006). One-to-one coupling of glacial climate variability in Greenland and Antarctica. *Nature*, *444*(7116), 195-198.
17. Ferrari, R., Jansen, M. F., Adkins, J. F., Burke, A., Stewart, A. L., & Thompson, A. F. (2014). Antarctic sea ice control on ocean circulation in present and glacial climates. *Proceedings of the National Academy of Sciences*, *111*(24), 8753-8758.

18. Gersonde, R., Crosta, X., Abelmann, A., & Armand, L. (2005). Sea-surface temperature and sea ice distribution of the Southern Ocean at the EPILOG Last Glacial Maximum—a circum-Antarctic view based on siliceous microfossil records. *Quaternary Science Reviews, 24*(7), 869-896.
19. Gottschalk, J., Battaglia, G., Fischer, H., Frölicher, T. L., Jaccard, S. L., Jeltsch-Thömmes, A., . . . Stocker, T. F. (2019). Mechanisms of millennial-scale atmospheric CO2 change in numerical model simulations. *Quaternary Science Reviews, 220*, 30-74. doi:https://doi.org/10.1016/j.quascirev.2019.05.013
20. Jaccard, S. L., Galbraith, E. D., Martínez-García, A., & Anderson, R. F. (2016). Covariation of deep Southern Ocean oxygenation and atmospheric CO2 through the last ice age. *Nature, 530*(7589), 207–210.
21. Jouzel, J., Delaygue, G., Amaeelle, L., Valerie, M.-D., Risi, C., & Vimeux, F. (2013). Water isotopes as tools to document oceanic sources of precipitation. *Water Resources Research, 49*(11), 7469-7486.
22. Kawamura, K., Parrenin, F., Lisiecki, L., Uemura, R., Vimeux, F., Severinghaus, J. P., . . . Jouzel, J. (2007). Northern Hemisphere forcing of climatic cycles in Antarctica over the past 360,000 years. *Nature, 448*(7156), 912-916.
23. Kindler, P., Guillevic, M., Baumgartner, M. F., Schwander, J., Landais, A., & Leuenberger, M. (2014). Temperature reconstruction from 10 to 120 kyr b2k from the NGRIP ice core. *Climate of the Past, 10*(2), 887-902.
24. Landais, A., Masson-Delmotte, V., Stenni, B., Selmo, E., Roche, D. M., Jouzel, J., . . . Arzel, O. (2015). A review of the bipolar see–saw from synchronized and high resolution ice core water stable isotope records from Greenland and East Antarctica. *Quaternary Science Reviews, 114*, 18-32.
25. Levermann, A., Schewe, J., & Montoya, M. (2007). Lack of bipolar see-saw in response to Southern Ocean wind reduction. *Geophysical Research Letters, 34*(34), 195-225.
26. Marcott, S. A., Bauska, T. K., Buizert, C., Steig, E. J., Rosen, J. L., Cuffey, K. M., . . . Kalk, M. L. (2014). Centennial-scale changes in the global carbon cycle during the last deglaciation. *Nature, 514*(7524), 616–619.
27. Margari, V., Skinner, L. C., Tzedakis, P. C., Ganopolski, A., Vautravers, M., & Shackleton, N. J. (2010). The nature of millennial-scale climate variability during the past two glacial periods. *Nature Geoscience, 3*(2), 127-131.
28. Mcmanus, J. F., Oppo, D. W., & Cullen, J. L. (1999). A 0.5-Million-Year Record of Millennial-Scale Climate Variability in the North Atlantic. *Science, 283*(5404), 971-975.

29. Menviel, L., Spence, P., & England, M. H. (2015). Contribution of enhanced Antarctic Bottom Water formation to Antarctic warm events and millennial-scale atmospheric CO2 increase. *Earth and Planetary Science Letters, 413*, 37-50.
30. Menviel, L., Spence, P., Yu, J., Chamberlain, M. A., Matear, R. J., Meissner, K. J., & England, M. H. (2018). Southern Hemisphere westerlies as a driver of the early deglacial atmospheric CO 2 rise. *Nature communications, 9*(1), 2503.
31. Munday, D. R., Johnson, H. L., & Marshall, D. P. (2013). Eddy saturation of equilibrated circumpolar currents. *Journal of Physical Oceanography, 43*(3), 507-532.
32. Nehrbass-Ahles, C., Shin, J., Schmitt, J., Bereiter, B., Joos, F., Schilt, A., . . . Grilli, R. (2020). Abrupt CO2 release to the atmosphere under glacial and early interglacial climate conditions. *Science, 369*(6506), 1000-1005.
33. NGRIP. (2004). High-resolution record of Northern Hemisphere climate extending into the last interglacial period. *Nature, 431*(7005), 147–151.
34. Nielsen, S. B., Jochum, M., Pedro, J. B., Eden, C., & Nuterman, R. (2019). Two - Timescale Carbon Cycle Response to an AMOC Collapse. *Paleoceanography and Paleoclimatology, 34*(4), 511-523.
35. Pedro, J. B., Jochum, M., Buizert, C., He, F., Barker, S., & Rasmussen, S. O. (2018). Beyond the bipolar seesaw: Toward a process understanding of interhemispheric coupling. *Quaternary Science Reviews, 192*, 27-46.
36. Rasmussen, S. O., Bigler, M., Blockley, S. P., Blunier, T., Buchardt, S. L., Clausen, H. B., . . . Fischer, H. (2014). A stratigraphic framework for abrupt climatic changes during the Last Glacial period based on three synchronized Greenland ice-core records: refining and extending the INTIMATE event stratigraphy. *Quaternary Science Reviews, 106*, 14-28.
37. Rhodes, R. H., Brook, E. J., Chiang, J. C., Blunier, T., Maselli, O. J., Mcconnell, J. R., . . . Severinghaus, J. P. (2015). Paleoclimate. Enhanced tropical methane production in response to iceberg discharge in the North Atlantic. *Science, 348*(6238), 1016-1019.
38. Skinner, L., Menviel, L., Broadfield, L., Gottschalk, J., & Greaves, M. (2020). Southern Ocean convection amplified past Antarctic warming and atmospheric CO 2 rise during Heinrich Stadial 4. *Communications Earth & Environment, 1*(1), 1-8.

39. Stenni, B., Buiron, D., Frezzotti, M., Albani, S., Barbante, C., Bard, E., . . . Bonazza, M. (2011). Expression of the bipolar see-saw in Antarctic climate records during the last deglaciation. *Nature Geoscience, 4*(1), 46-49.
40. Stocker, T. F., & Johnsen, S. J. (2003). A minimum thermodynamic model for the bipolar seesaw. *Paleoceanography, 18*(4), 1087.
41. Stuut, J. B. W., Crosta, X., Borg, K. V. D., & Schneider, R. (2004). Relationship between Antarctic sea ice and southwest African climate during the late Quaternary. *Geology, 32*(10), 909-912.
42. Svensson, A., Andersen, K. K., Bigler, M., Clausen, H. B., Dahljensen, D., Davies, S. M., . . . Rasmussen, S. O. (2008). A 60 000 year Greenland stratigraphic ice core chronology. *Climate of the Past Discussions, 3*(6), 47-57.
43. Svensson, A., Dahl-Jensen, D., Steffensen, J. P., Blunier, T., Rasmussen, S. O., Vinther, B. M., . . . Bigler, M. (2020). Bipolar volcanic synchronization of abrupt climate change in Greenland and Antarctic ice cores during the last glacial period. *Clim. Past, 16*(4), 1565-1580. doi:10.5194/cp-16-1565-2020
44. Thompson, A. F., Hines, S. K., & Adkins, J. F. (2019). A Southern Ocean Mechanism for the Interhemispheric Coupling and Phasing of the Bipolar Seesaw. *Journal of Climate, 32*(14), 4347-4365.
45. Toggweiler, J. R., Russell, J. L., & Carson, S. R. (2006). Midlatitude westerlies, atmospheric CO2, and climate change during the ice ages. *Paleoceanography, 21*(2), PA2005.
46. Veres, D., Bazin, L., Landais, A., Toyé Mahamadou Kele, H., Lemieux-Dudon, B., Parrenin, F., . . . Capron, E. (2013). The Antarctic ice core chronology (AICC2012): an optimized multi-parameter and multi-site dating approach for the last 120 thousand years. *Climate of the Past, 9*(4), 1733-1748.
47. WAIS, D. P. M. (2013). Onset of deglacial warming in West Antarctica driven by local orbital forcing. *Nature, 500*(7463), 440-444.
48. WAIS, D. P. M. (2015). Precise interpolar phasing of abrupt climate change during the last ice age. *Nature, 520*(7549), 661-665.
49. Watanabe, O., Jouzel, J., Johnsen, S., Parrenin, F., Shoji, H., & Yoshida, N. (2003). Homogeneous climate variability across East Antarctica over the past three glacial cycles. *Nature, 422*(6931), p. 509-512.
50. Wolff, E. W., Fischer, H., & Röthlisberger, R. (2009). Glacial terminations as southern warmings without northern control. *Nature Geoscience, 2*(3), 206-209.

References From the Supporting Information

51. Ahn, J., Headly, M., Wahlen, M., Brook, E. J., Mayewski, P. A., & Taylor, K. C. (2008). CO 2 diffusion in polar ice: observations from naturally formed CO 2 spikes in the Siple Dome (Antarctica) ice core. *Journal of Glaciology*, *54*(187), 685-695.
52. Bereiter, B., Eggleston, S., Schmitt, J., Nehrbass Ahles, C., Stocker, T. F., Fischer, H., . . . Chappellaz, J. (2015). Revision of the EPICA Dome C CO2 record from 800 to 600 kyr before present. *Geophysical Research Letters*, *42*(2), 542-549.
53. Bereiter, B., Lüthi, D., Siegrist, M., Schüpbach, S., Thomas F, S., & Fischer, H. (2012). Mode change of millennial CO2 variability during the last glacial cycle associated with a bipolar marine carbon seesaw. *Proceedings of the National Academy of Sciences of the United States of America*, *109*(25), 9755-9760.
54. Buizert, C., Sigl, M., Severi, M., Markle, B. R., Wettstein, J. J., McConnell, J. R., . . . Kawamura, K. (2018). Abrupt ice-age shifts in southern westerly winds and Antarctic climate forced from the north. *Nature*, *563*(7733), 681-685.
55. EPICA. (2004). Eight glacial cycles from an Antarctic ice core. *Nature*, *429*(6992), 623-628.
56. Landais, A., Masson-Delmotte, V., Stenni, B., Selmo, E., Roche, D. M., Jouzel, J., . . . Arzel, O. (2015). A review of the bipolar see–saw from synchronized and high resolution ice core water stable isotope records from Greenland and East Antarctica. *Quaternary Science Reviews*, *114*, 18-32.
57. Nehrbass-Ahles, C., Shin, J., Schmitt, J., Bereiter, B., Joos, F., Schilt, A., . . . Grilli, R. (2020). Abrupt CO2 release to the atmosphere under glacial and early interglacial climate conditions. *Science*, *369*(6506), 1000-1005.
58. Stenni, B., Buiron, D., Frezzotti, M., Albani, S., Barbante, C., Bard, E., . . . Bonazza, M. (2011). Expression of the bipolar see-saw in Antarctic climate records during the last deglaciation. *Nature Geoscience*, *4*(1), 46-49.
59. Svensson, A., Andersen, K. K., Bigler, M., Clausen, H. B., Dahljensen, D., Davies, S. M., . . . Rasmussen, S. O. (2008). A 60 000 year Greenland stratigraphic ice core chronology. *Climate of the Past Discussions*, *3*(6), 47-57.
60. Veres, D., Bazin, L., Landais, A., Toyé Mahamadou Kele, H., Lemieux-Dudon, B., Parrenin, F., . . . Capron, E. (2013). The Antarctic ice core chronology (AICC2012): an optimized multi-parameter and multi-site dating approach for the last 120 thousand years. *Climate of the Past*, *9*(4), 1733-1748.

Geophysical Research Letters

Supporting Information for

Different trends in Antarctic temperature and atmospheric CO_2 during the last glacial

Peisong Zheng[1, 2], Joel B. Pedro[3,4], Markus Jochum[5], Sune O. Rasmussen[6], Zhongping Lai[1, 7 *]

[1] Guangdong Provincial Key Laboratory of Marine Biotechnology, Institute of Marine Sciences, Shantou University, Shantou 515063, China.

[2] School of Earth Sciences, China University of Geosciences, Wuhan 430074, China.

[3] Australian Antarctic Division, Kingston, Tasmania, Australia.

[4] Australian Antarctic Program Partnership, University of Tasmania, Hobart, Tasmania, Australia.

[5] TeamOcean, Niels Bohr Institute, University of Copenhagen, Copenhagen, Denmark.

[6] Centre for Ice and Climate, Section for the Physics of Ice, Climate, and Earth, Niels Bohr Institute, University of Copenhagen, Copenhagen, Denmark.

[7] Three Gorges Research Center for Geohazards of MOE, China University of Geosciences, Wuhan 430074, China.

Contents of this file

Introduction

This document presents the supporting material for the temperature and CO_2 results. In Text S1 we discussed the sensitivity of the observed difference between CO_2 and Antarctic temperature to the influence of gas diffusion, ice diffusion, the choice of timescale, and the varying delta-age. The results support our conclusion in the main text.

Figure S1 to S4 and Table S1 are supporting information for temperature results, Figure S1 shows the 'temperature overshoot', Figure S2 to S4, and Table S1 show the exponential fit for the AIMs and the analysis results for individual ice cores of the five-core averaged data. Figure S5 to S12 show the searched maximums/minimums for different CO_2 records, the significant test for the nHS CO_2 amplitude, and the results of CO_2 sensitivity test.

Text S1. Sensitivity test for CO_2 results

Three main factors can unevenly smooth the CO_2 record and influence the CO_2 amplitude and rate, the first is the varying resolution, with lower resolution reducing the CO_2 amplitude. The second is the different firn diffusion and enclosure characteristics between ice core sites (Bereiter et al., 2012). The third is the diffusion in ice (Ahn et al., 2008), which unevenly smooth CO_2 in different depths, with deeper ice being smoothed more (Ahn et al., 2008).

For the influence of varying resolution, the 300 yr window we applied for moving averages is larger than the 88% quantile of the resolution of MIS-3 section of composite CO_2 data, thus it is capable to reduce the effect of varying resolution by removing the

high-frequency signal. Our conclusion also holds when the smoothing length increased to 500 yr (Figure S12), suggest the varying record resolution has negligible influence on our finding.

To evaluate the influence of different enclosure characteristics between ice cores, we performed a one to one comparison for the trend of Talos CO_2 data (in AICC2012 timescale; Bereiter et al., 2012, 2015) and Talos $\delta^{18}O$ data (in AICC2012 timescale; Figure S8; Landais et al., 2015; Stenni et al., 2011; Veres et al., 2013), both records are smoothed by 300 yr moving average before searching maximums/minimums. Due to the uneven spacing between Greenland climate transition (in GICC05 timescale; Rasmussen et al., 2014) and the AIM peaks/valleys of the Talos $\delta^{18}O$, we manually determined the $\delta^{18}O$ maximums and minimums. The CO_2 maximums/minimums are directly searched in the smoothed data by the same method as the main text. The two-side significance of the BPS warming rate slope is 85.09%, probably due to reduced event numbers. But it is still significantly higher than the two-side significance of CO_2 slope, which is only 54.44% (Figure S8), The result thus supports the conclusion that the CO_2 trend is less sensitive to varying background climate than the temperature trend and indicates the site-dependent gas diffusion does not change our conclusion.

The result also shows the varying of delta-age between gas and ice does not change our conclusion. As the BPS warming rate in Talos $\delta^{18}O$ is calculated in GICC05 timescale (Svensson et al., 2008), and the CO_2 timescale is synchronized to it by CH_4 synchronization (Veres et al., 2013). Thus, the influence of delta-age is largely reduced in this experiment.

To evaluate the influence of depth/time-dependent ice diffusion, we compared the MIS-3 CO_2 amplitudes with the one from the newly recovered high-resolution (ca. 200 yr) EDC CO_2 data of MIS-10, 11, and 12 (in AICC2012 timescale, Figure S9, S10; Nehrbass-Ahles et al., 2020). The EDC CO_2 amplitudes are in line with Talos (Figure S10), suggesting that the CO_2 amplitude is not significantly reduced due to ice diffusion. Moreover, we compared the trend between new EDC CO_2 with the EDC δD (in AICC2012 timescale, Figure S9, the CO_2/δD maximums and minimums are manually determined from the 300 yr smoothed data), the two-side significance of CO_2 and temperature rate slope is 58.55% and 89.20% respectively, support our conclusion and indicate the influence of ice diffusion is negligible. The result also suggests the different CO_2 and Antarctic temperature trend exist beyond the last ice age.

The above experiments also suggest the different CO_2 and Antarctic temperature sensitivity to varying background climate is not biased by the use of timescale, as our results show high consistency between different combinations of records: composite CO_2 data (AICC2012) vs five core averaged $\delta^{18}O$ (WD2014), Talos CO_2 (AICC2012) vs Talos $\delta^{18}O$ (GICC05); EDC CO_2 data (AICC2012) vs EDC δD data (AICC2012).

To further test the robustness of our conclusion we also used alternative Methods to compare the slopes of CO_2 and temperature rates: in each iteration, for each CO_2/temperature rate, we draw values from their normal distribution defined by their value with standard deviation set as their 1-sigma uncertainty. Then we normalized the randomly generated CO_2/temperature rates to zero mean and unit variance separately and linear fit the AIM age against the rates and record the fitted slope. After 100,000

iterations, we compare the distribution of the slope of CO_2 and temperature rates. For all three combinations: five-core average $\delta^{18}O$ vs composite CO_2 data, Talos CO_2 vs Talos $\delta^{18}O$, and new EDC CO_2 data vs EDC δD, the median temperature rate slope is larger than the CO_2 rate slope (Figure 3e, 3f, S11). This result is supported by a t-test that shows the CO_2 and temperature rate slope are significantly different (at 95% significance level) in all three cases.

We also explored whether our results are sensitive to the change in smoothing Methods, or the use of detrended data (composite CO_2 data is used, with all 10 events). When the detrended CO_2 data is used (created by removing the long-term signal, represented by the 20,000 yr moving average smoothing, from the composite CO_2 record), the two-side significance for the slope of CO_2 rate is 85.99% (Figure S12). We create a spline-fitted CO_2 record by fitting the composite CO_2 record by smooth spline with cut-off period of 500 yr (Bereiter et al., 2012). The two-side significance of the slope of CO_2 rates is 89.62% (Figure S12). In both cases, the two-side significance of the CO_2 rate slope is similar to what we reported in the main text, and the significant difference between HS and nHS CO_2 rate is not detected (by t-test, at 95% significance level), a significant difference between HS and nHS CO_2 overshoots are confirmed (by t-test, at 95% significance level).

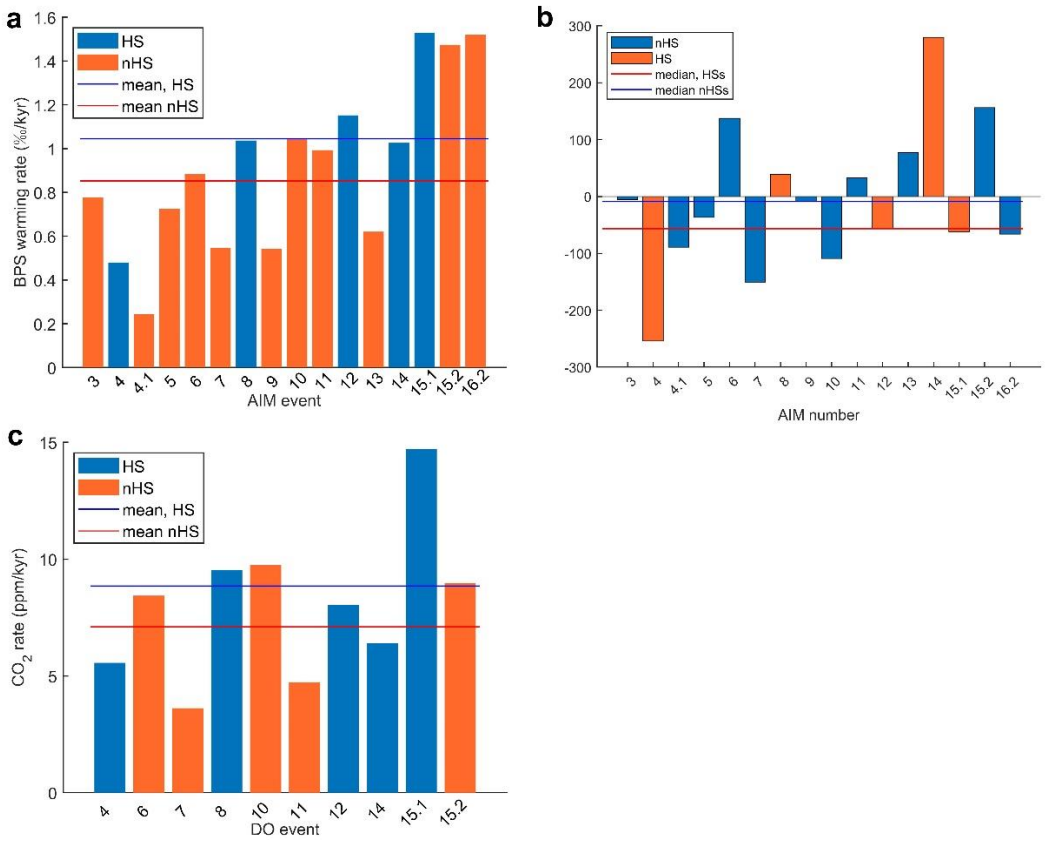

Figure S1. The bar chart for the rate and time of temperature and CO_2 rise. **a.** The BPS warming rates. **b**. the Antarctic warming overshoot. **c.** CO_2 rates.

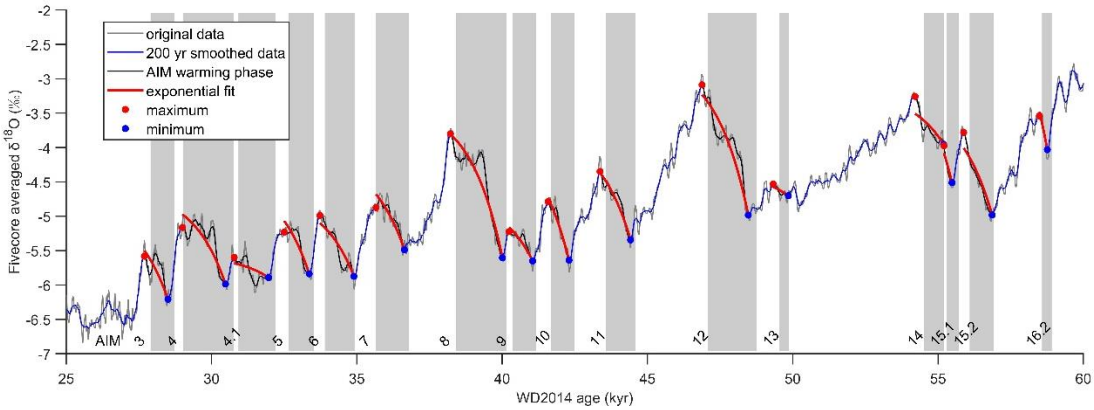

Figure S2. The exponential fit for the AIMs on the five-core averaged data (Buizert et al., 2018). Gray vertical bars mark the Greenland stadials.

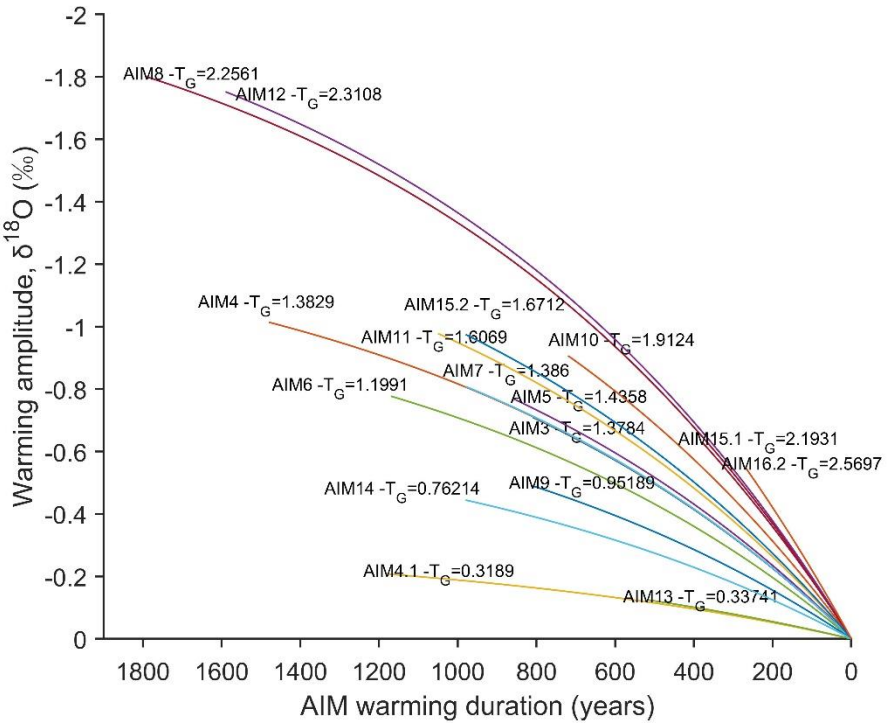

Figure S3. Comparison of the $-T_G$ of the AIMs. The $-T_G$ is calculated from the five-core averaged data (Buizert et al., 2018).

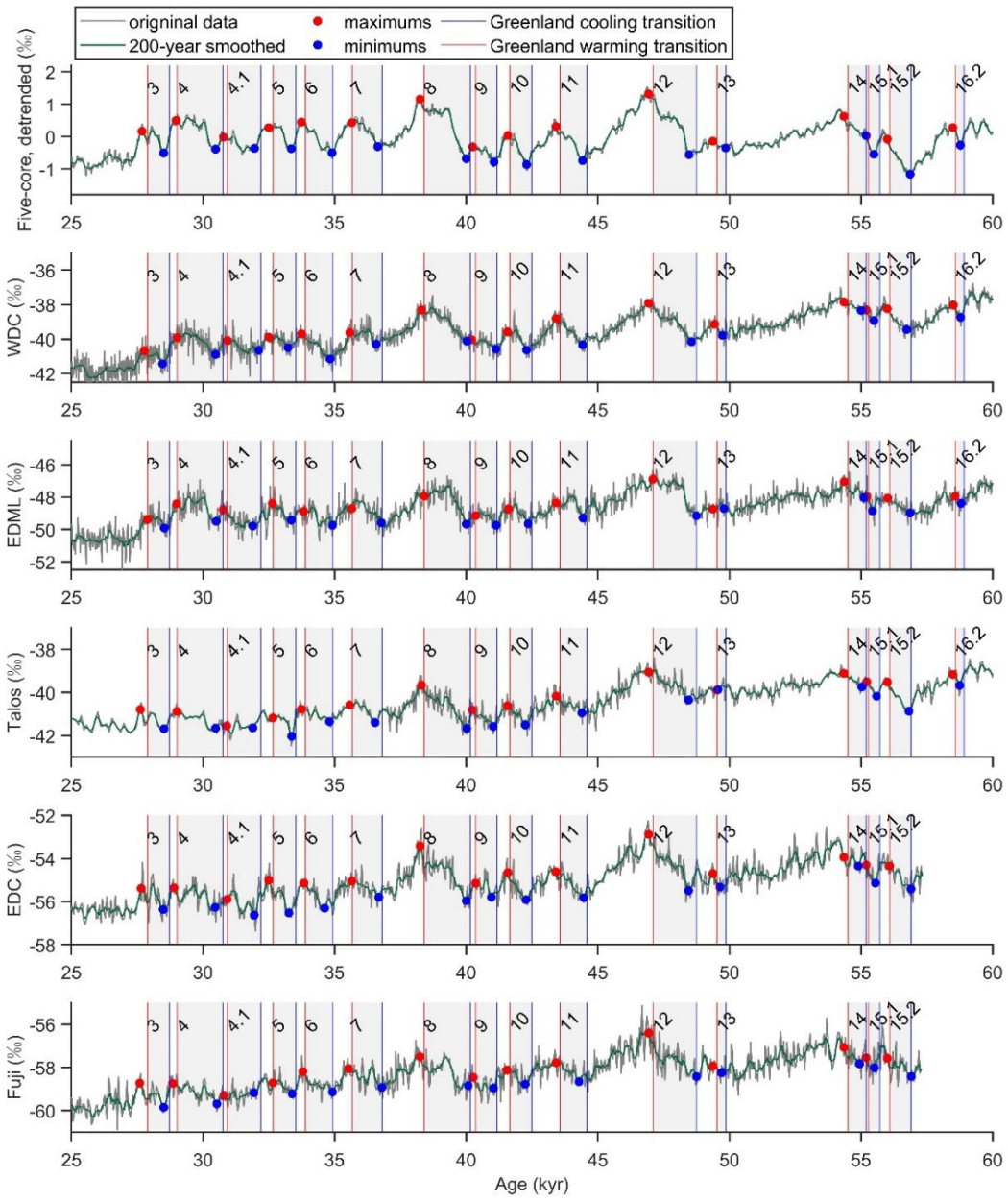

Figure S4. Example for the searched maximums and minimums. From top to bottom: the detrended five-core averaged data (Buizert et al., 2018), West Antarctic Ice Sheet Divide (WDC; WAIS, 2013, 2015), European Project for Ice Coring in Antarctica (EPICA) in the interior of Dronning Maud Land (EDML; EPICA, 2006), Talos Dome (Landais et al., 2015; Stenni et al., 2011), EPICA Dome C (EDC; EPICA 2004), and Dome Fuji (Fuji; Kawamura et

al., 2007; Watanabe et al., 2003). All these ice cores are on WD2014 time scale(Buizert et al., 2018).

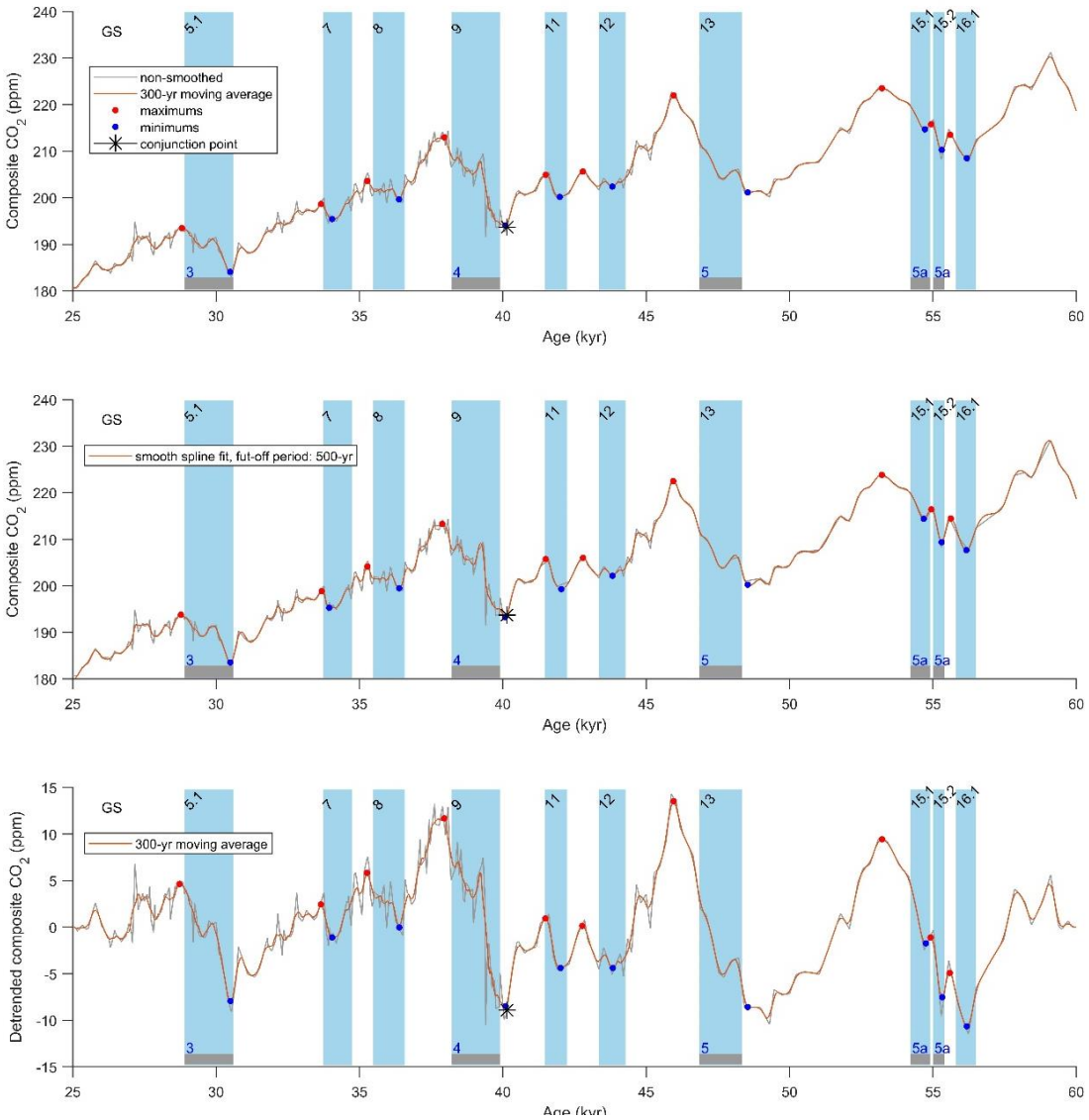

Figure S5. Example of the maximums and minimums searched in the CO_2 records. From top to bottom: the composite CO_2 (Bereiter et al., 2012), smooth spline fitted composite CO_2 data, and the detrend composite CO_2 data. The time of Greenland stadial and Heinrich events are marked by blue and gray bars respectively.

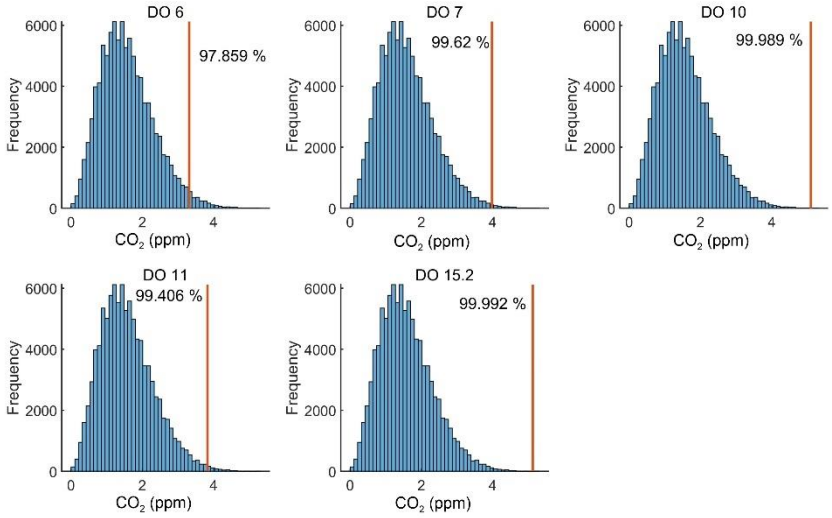

Figure S6. The significance of the CO_2 amplitude for the nHSs. For all five events, the amplitude of CO_2 rise is significantly larger than the uncertainty of amplitude (in 95% level). Here the distribution of the uncertainty of amplitude is calculated by adding the uncertainty of two arbitrarily selected CO_2 data points in the composite CO_2 record and repeat the operation100,000 times.

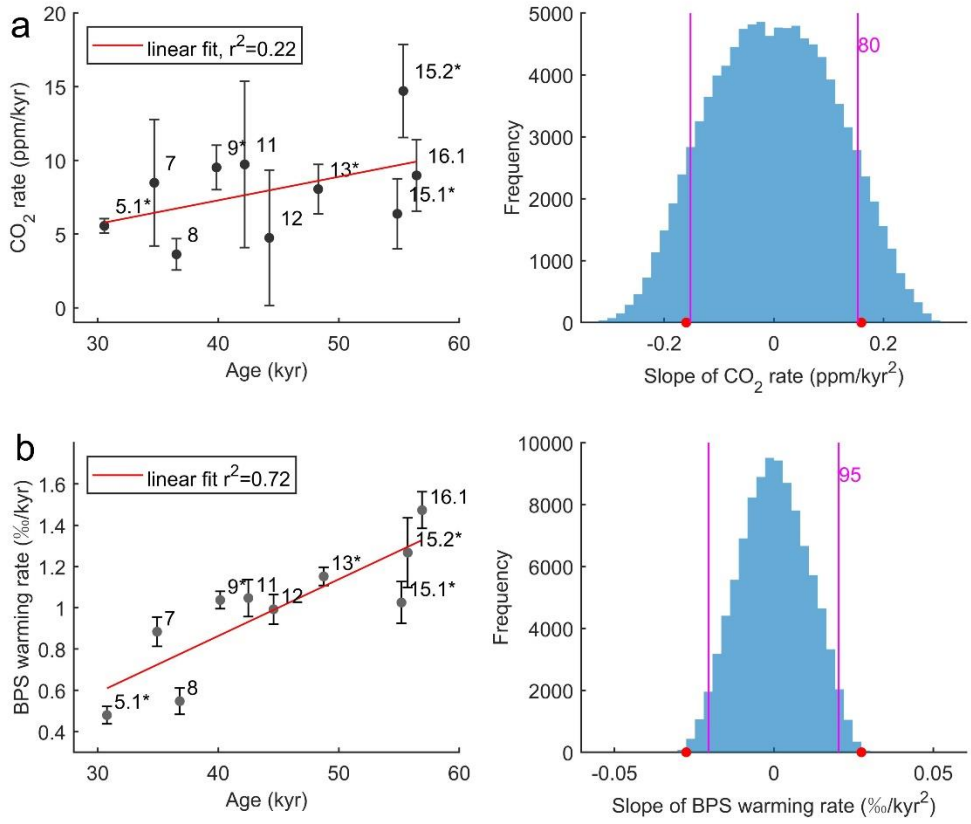

Figure S7. Comparison of CO_2 and temperature trend of composite CO_2 data (Bereiter et al., 2015) and Antarctic five-core average $\delta^{18}O$ (Buizert et al., 2018) for the same GSs. **a.** The CO_2 rate plot against the age of corresponding GS (left); the two-side significance of the CO_2 rate slope calculated from randomly permuting the CO_2 rate 100,000 times (right). The error bar in the left shows the 95% CI of the CO_2 rate from the MC simulation. **b.** Same as **a** but for five-core average $\delta^{18}O$ data. The two-side significance of the CO_2 and warming rate slope are 82.43% and 99.87% respectively.

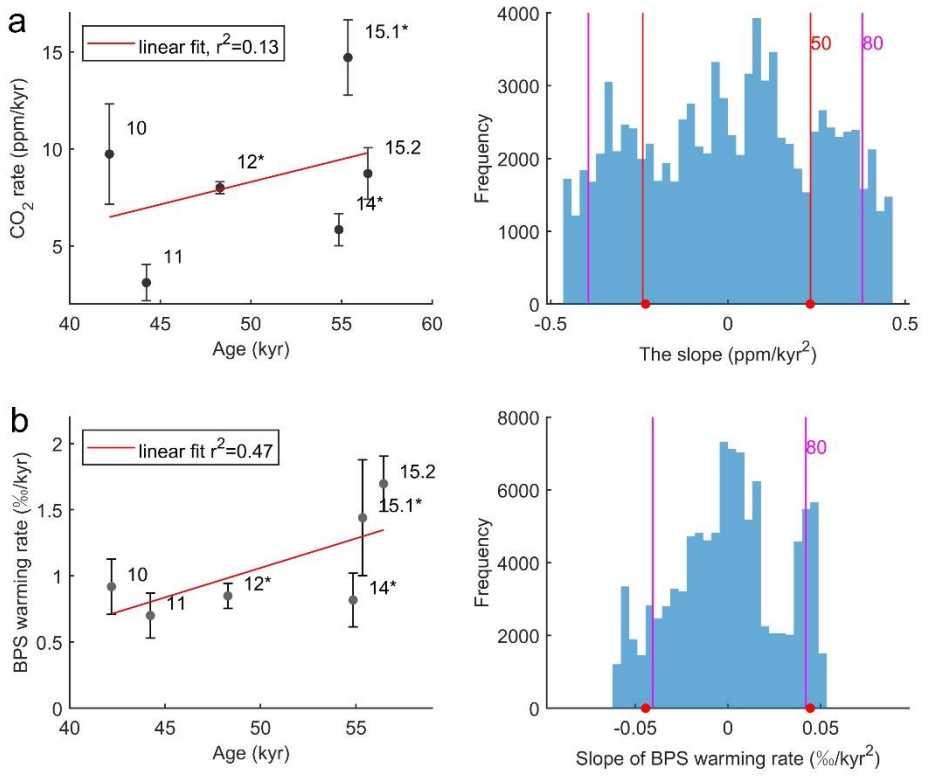

Figure S8. Comparison of Talos Dome CO_2 and temperature trend. **a.** The CO_2 rate plot against the age of corresponding GS (left); the two-side significance of the CO_2 rate slope (right). The uncertainty of the CO_2 rate in the left is derived from the uncertainty of the amplitude, which is the sum of the corresponding uncertainty of maximums and minimums (interpolated from the uncertainty of CO_2 data at the time of maximums/minimums; Bereiter et al., 2015; Bereiter et al., 2012). **b.** Same as **a** but for Talos $\delta^{18}O$ data (Landais et al., 2015; Stenni et al., 2011). The uncertainty of the warming rate is derived from the uncertainty of the amplitude, and the uncertainty of $\delta^{18}O$ maximums and minimums are set as the standard deviation of the residual, which is the isotope difference between the unsmoothed and 300 yr smoothed data.

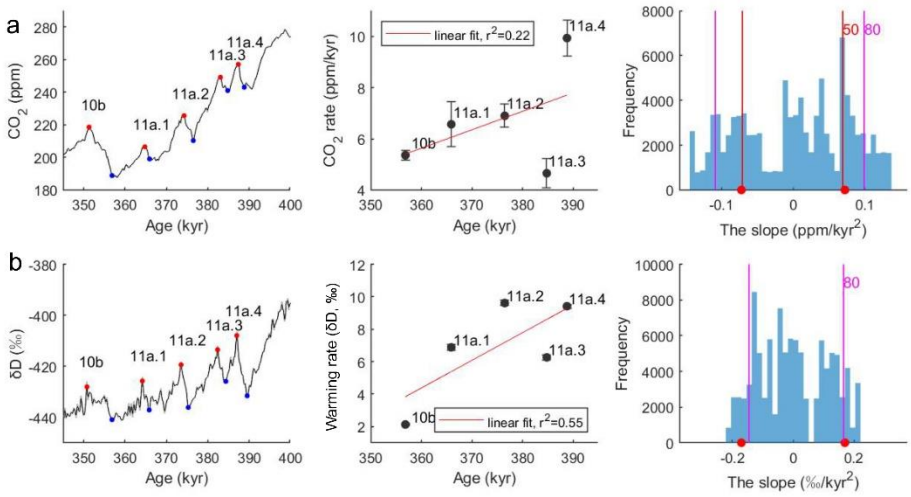

Figure S9. Comparison of EPICA Dome C CO_2 and temperature trend during 350 to 400 kyr BP. **a.** The CO_2 maximums and minimums manually picked in the 300 yr moving average smoothed new EDC CO_2 data (Nehrbass-Ahles et al., 2020) (left), the uncertainty of the maximums/minimums are interpolated from the uncertainty of CO_2 data (Nehrbass-Ahles et al., 2020) at the time of maximums/minimums; The CO_2 rate plotted against the age of CO_2 rise (defined as the age of corresponding CO_2 minimum, middle), the uncertainty of the CO_2 rate is derived from the uncertainty of the amplitude; the two-side significance of the CO_2 rate slope (right). **b.** Same as **a** but for EDC δD data (EPICA, 2004). The uncertainty of the maximums and minimums are set as the standard deviation of the residual, the residual is the δD difference between the unsmoothed and 300 yr smoothed data. We identified the CO_2 and temperature rise with the corresponding carbon dioxide maximum labeled by previous research (Nehrbass-Ahles et al., 2020). The CO_2 and δD record are both in AICC2012 timescale.

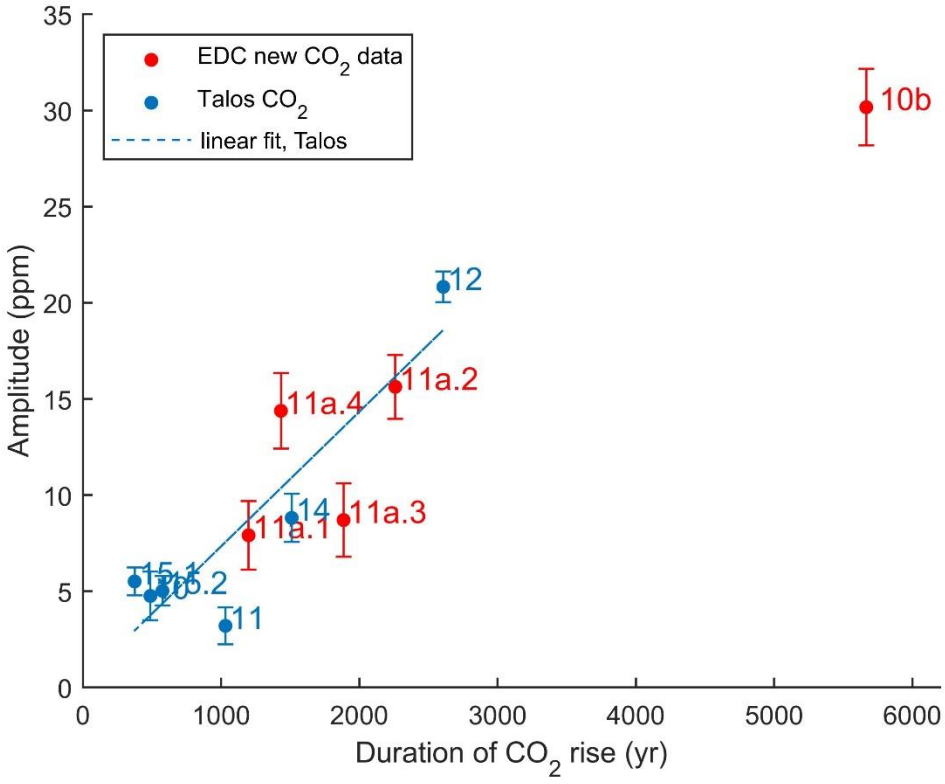

Figure S10. Comparison of the amplitude of CO_2 rise of Talos CO_2 data (Bereiter et al., 2012) and the new EDC CO_2 data (Nehrbass-Ahles et al., 2020). The CO_2 rises in new EDC data are labeled in their corresponding CO_2 maximum following previous research (Nehrbass-Ahles et al., 2020).

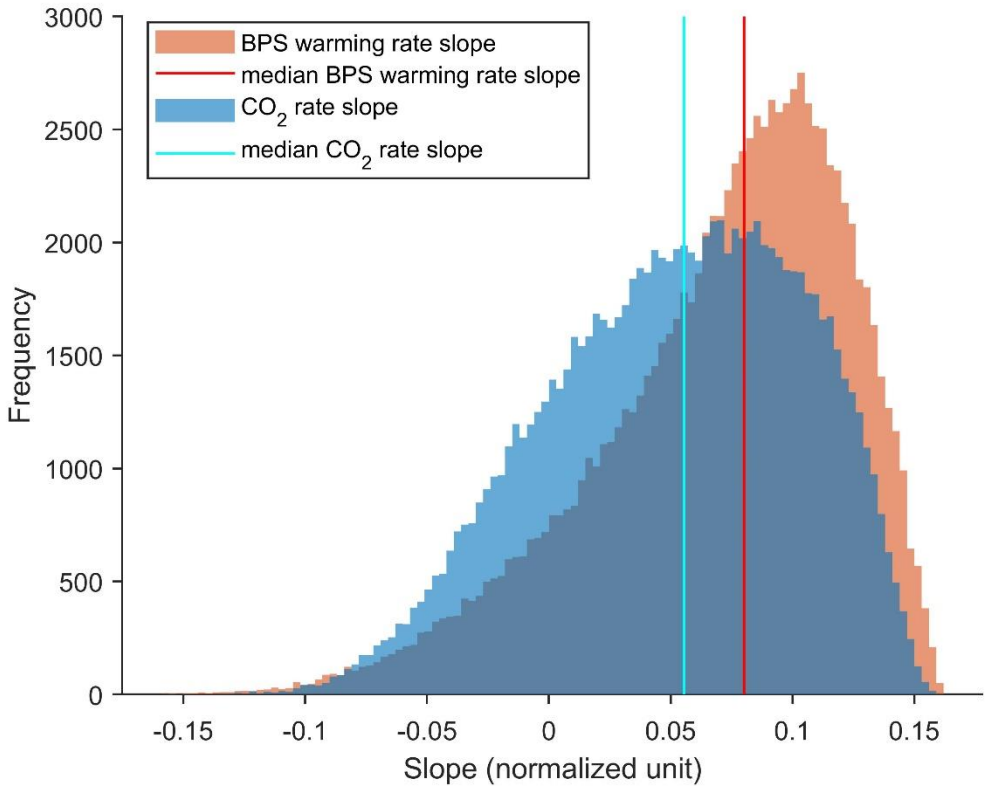

Figure S11. The distribution of randomly generated CO_2 and temperature rate slope for the Talos data. The CO_2 data is from (Bereiter et al., 2012), the $\delta^{18}O$ data is from (Landais et al., 2015; Stenni et al., 2011). The randomly generated rates have been normalized to zero mean and unit variance before linear fit to calculate the slope.

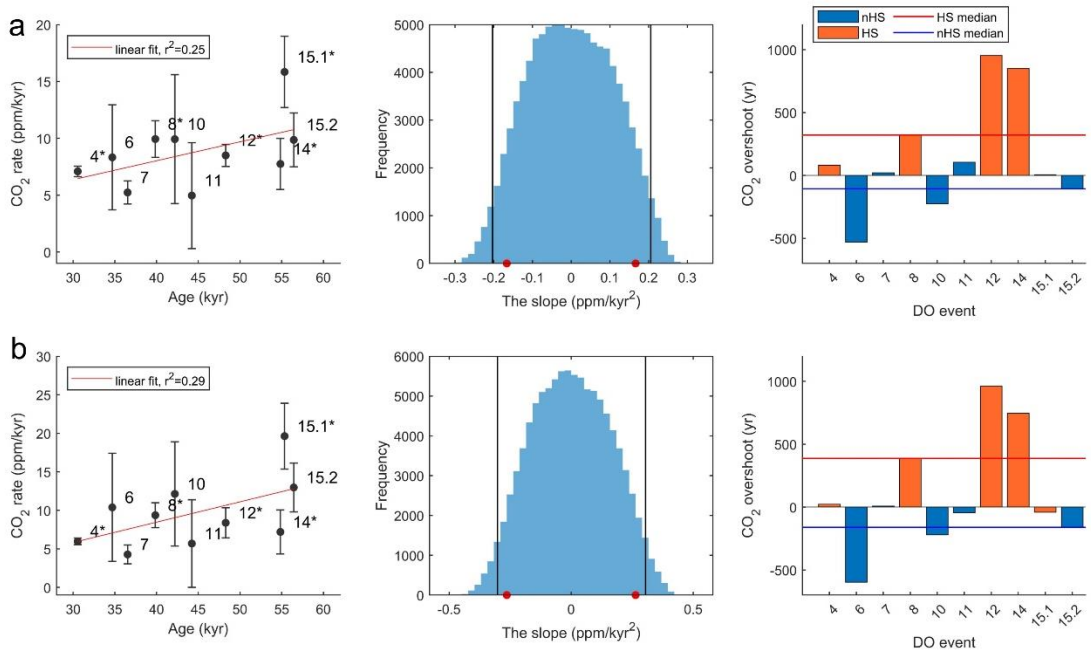

Figure S12. CO_2 results from the detrended and smooth spline fitted composite CO_2 data (Bereiter et al., 2015). **a.** results for detrend data: CO_2 rate plotted against the age of the corresponding AIM (left), error bar show the 95% CI; two-side significance for the slope of the CO_2 rates, the vertical black lines mark the 95% confidence level (middle); The CO_2 overshoot (right). **b.** same as **a** but for the smooth spline fitted data, with cut-off period of 500 yr (Bereiter et al., 2012).

Record	1 sigma uncertainty of MC simulation (‰)	Significance of two-side, BPS warming rate slope (%)	t-test, HS vs nHS BPS warming rate (1 for significant 0 for not significant)	Significance of two-side, warming rate slope (%), Antarctic perspective	t-test, HS vs nHS warming rate (1 or 0), Antarctic perspective	two side significance of the -T_G slope (%)
Five-core Antarctic perspective	0.12	–	–	99.65	0	–
Five-core detrended	0.12	99.98	0	99.40	0	94.59
WDC $\delta^{18}O$	0.36	99.94	0	99.91	0	–
EDML $\delta^{18}O$	0.43	99.92	0	98.37	0	–
Talos $\delta^{18}O$	0.30	99.92	0	99.49	0	–
EDC $\delta^{18}O$	0.33	98.73	0	96.37	0	–
Fuji $\delta^{18}O$	0.33	97.62	0	99.89	0	–

Table S1. The analysis results for the AIM warming from Antarctic perspective, the detrended five-core averaged data, and the individual ice cores that go into the five-core averaged data (Buizert et al., 2018). Note that the two-side significance for the -T_G slope for the detrended data is slightly below the threshold we set, but as the value is very high, we still suggest a significantly lowered -T_G throughout the MIS-3. The exponential fit and -T_G calculation for the individual ice cores of the five-core averaged record is impeded by the high noise level.